Development of ScAlN PMUTs for Medical Applications

Cyril Baby Karuthedath, Abhilash Thanniyil Sebastian, Panu Helistö, Teuvo Sillanpää, and Anu Kärkkäinen

***Abstract*— In this paper, the design, fabrication and characterization of PMUTs for medical applications are discussed. Scandium (20% Sc/(Sc+Al)) doped AlN is used as the piezoelectric material. The fabrication process for PMUTs with a patterned piezoelectric layer is developed. Single-cell and linear arrays of PMUT are fabricated and electrical, mechanical and acoustic characterization is carried out. The piezo-patterning improved the performance of PMUTs. The fabricated PMUT showed excellent chip-wafer level uniformity and yield. At resonance (5.7 MHz), the ScAlN PMUT array showed transmit sensitivity of 13 kPa/V and receive sensitivity of 1.1 V/MPa. The good transmit-receive properties and the ability to operate without bias voltage make the ScAlN PMUTs best for voltage-limited medical applications. [2023-0131]**

***Index Terms*— PMUT, ScAlN, cavity silicon on insulator (CSOI), medical ultrasound.**

I. Introduction

MICROMACHINED Ultrasonic Transducers (MUTs) offer several advantages over conventional ceramic piezoelectric transducers widely used in medical ultrasonic devices [1]. This includes miniature size, wider frequency range, better coupling to medium, larger bandwidth, easy fabrication of multi-dimensional arrays, CMOS compatibility and mass production capability. The advancement in microfabrication technology drives the development of high performance Capacitive and Piezoelectric MUTs. CMUTs are based on capacitive actuation and sensing mechanisms, while the PMUTs utilize piezoelectric mechanisms for transduction. Compared to PMUT, CMUT is a well-researched and mature technology. Commercial medical devices using CMUTs are available on the market [2], [3]. The requirement of a high DC bias voltage (in the range of 70-140 V) for its operation limits the application of the CMUTs.

The ability of PMUT to operate without DC bias voltage makes it attractive for voltage and power-limited medical applications such as wearables [4], [5], implantables [6], etc. This, together with the recent advancements in piezoelectric thin films, has enabled the rapid developed of PMUT technology in the last decade. Lead zirconate titanate (PZT) and Aluminum Nitride (AlN) are the most commonly used piezo materials for PMUTs [7], [8], [9]. PZT PMUT offers very good transmit performance because of the large piezoelectric coefficient. On the other hand, the large dielectric constant of PZT leads to poor receive sensitivity. Furthermore, PZT requires a high processing temperature and is non-compatible with CMOS processes. Owing to the low dielectric constant, AlN-based PMUT has better receive performance. AlN PMUTs are also CMOS compatible. However, the low piezoelectric coefficient of AlN results in poor transmit performance. It has been shown that the piezoelectric coefficient of AlN can be improved by doping with Sc, without compromising the receive performance and CMOS compatibility [10], [11], [12]. ScAlN is a relatively new piezoelectric material and the potential of ScAlN PMUT is not fully explored.

The design, fabrication and characterization of a piezo-etched ScAlN based PMUTs are discussed in the paper. The PMUTs are developed to be used in an ultrasonic wearable patch for medical applications. An example of such application is continuous monitoring of blood pressure [13]. Ultrasound-based blood pressure measurement is a non-invasive technique that measures change in diameter to determine the blood pressure. The diameter of the artery is typically measured from the reflections of the ultrasound signal from the arterial walls. The change in diameter is then used to estimate changes in blood pressure based on the Polakowski formula, which relates arterial diameter to blood pressure [14]. While the paper examines the feasibility of using ScAlN PMUT in wearable applications, demonstrating its application is outside the scope of the paper.

II. Design

A. PMUT Cell

PMUT is a clamped membrane that vibrates out of the planes to generate and sense ultrasound signals. The three-dimensional (3D) cross-section view of the water-coupled PMUT cell is shown in Figure 1. The membrane consists of a Silicon (Si) structural layer, 20% Scandium (Sc) doped AlN as piezoelectric material, and Molybdenum (Mo) as top and bottom electrodes. Layer thickness and membrane diameters are given in Table I. The cavity beneath the silicon structural layer is in vacuum conditions.

The proposed PMUT design differs from conventional water-coupled PMUTs [12] as it involves patterning the piezoelectric material. Specifically, in this design, the piezoelectric layer outside the electrode area is patterned. The piezoelectric layer only covers 70% of the total membrane surface area.

Manuscript received 11 July 2023; accepted 12 July 2023. Date of publication 28 July 2023; date of current version 3 October 2023. This work was supported in part of the ULIMPIA Project through PENTA under Grant PENTA-2017-Call2-16101-ULIMPIA (www.ulimpia-project.eu) and in part by Okmetic Oy for providing Cavity Silicon on Insulator (CSOI) wafers in the Electronic Components and Systems for European Leadership (ESCEL) Project Position II under Grant Ecsel-783132-Position-II-2017-IA. Subject Editor E. S. Kim. *(Corresponding author: Cyril Baby Karuthedath.)*

The authors are with the VTT Technical Research Centre of Finland Ltd., 02150 Espoo, Finland (e-mail: cyril.karuthedath@vtt.fi).

Color versions of one or more figures in this article are available at https://doi.org/10.1109/JMEMS.2023.3296159.

Digital Object Identifier 10.1109/JMEMS.2023.3296159

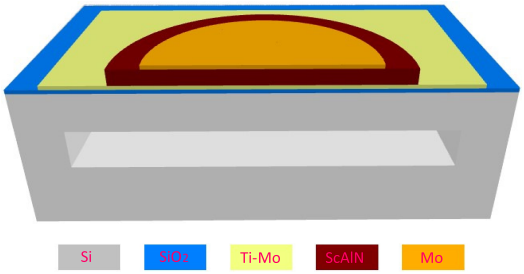

Fig. 1. 3D cross-sectional schematic of ScAlN PMUT.

TABLE I
PMUT LAYER THICKNESS AND MEMBRANE DIAMETER

Parameter	Dimension (μm)
Membrane diameter	90
Top electrode diameter	63
Piezoelectric layer diameter	63
Si structural layer thickness	4.5
ScAlN piezoelectric layer thickness	1
Top Mo electrode thickness	0.2
Bottom Mo electrode thickness	0.2

This differs from the pinned PMUT discussed in a previous study [15], where only a small region of the piezoelectric layer at the edge of the membrane clamping area was patterned. In the pinned structure, due to the higher aspect ratio of the membrane and the fact that the piezoelectric layer thickness is almost half of the membrane thickness, the patterning of the piezoelectric layer modified the mode shape. However, in the proposed piezoelectric design, since the piezoelectric layer thickness is much lower than the structural layer thickness, the effect of patterning on the mode shape of the membrane is expected to be less significant. It is important to note that the piezo-patterned PMUT structures discussed in the previous studies [15], [16] were air-coupled PMUTs, which typically operate at lower frequencies and have thinner and wider membranes compared to water-coupled PMUTs. Patterning of the piezoelectric layer in air-coupled PMUTs improved PMUT performance, but it also adds additional stress that could bend the membranes. Moreover, the piezo-patterned air-coupled PMUT is expected to be more sensitive to wafer-level stress variations. In air-coupled PMUTs, piezo patterning improved the PMUT performance, probably at the cost of wafer-level uniformity, which is not studied in the paper.

The piezo-patterned PMUT structure has several advantages. First, patterning the piezoelectric layer reduces the stiffness of the etched area of the membrane, increasing the displacement sensitivity and improving the transmit and receive performance of the PMUT. The dominant factors determining wafer-level uniformity in PMUTs are the membrane diameter variation, thickness variation, and stress variation of the sputtered films [17], [18]. In Cavity Silicon on Insulator (CSOI) based PMUTs, dimensional variation across the wafer is expected to be minimal, so the stress variation of the sputtered ScAlN, which is in the range of a few hundred MPa, and the Si thickness variation are the dominant factors. Patterning the piezo layer also releases stress and reduces the effect of piezoelectric stress variation on the membrane. In the proposed water-coupled design, since the thickness of the structural layer is higher than the piezoelectric layer, the additional stress introduced due to patterning is expected to be negligible. Therefore, piezo layer patterning is expected to improve chip and wafer-level uniformity in the proposed water-coupled PMUTs. Finally, as the thermal expansion coefficient of ScAlN is high, piezoelectric layer patterning improves the thermal stability of the PMUT, although this is not critical for water-coupled PMUTs [19].

TABLE II
MATERIAL PROPERTIES USED IN COMSOL SIMULATION MODEL

Property	ScAlN		Si	Mo	SiO_2
Density(kg/m^3)	3560		2320	10200	2200
Poisson ratio	0.177		0.22	0.31	0.17
Young's Modulus/ Elastic Stiffness matrix(GPa)	C_{11}	196	160	312	70
	C_{12}	761			
	C_{13}	68			
	C_{33}	225			
	C_{44}	67			
	C_{66}	63			
Peizoelectric Stress matrix(C/m^2)	e_{31}	-0.788	-	-	-
	e_{33}	2.038	-	-	-
	e_{15}	-6.522	-	-	-
Dielectric permittivity	12		-	-	-

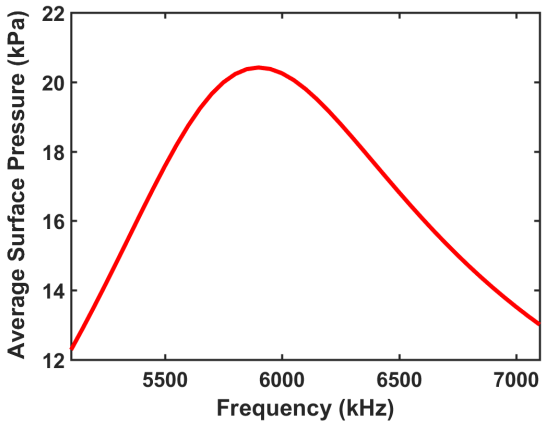

Fig. 2. Average surface pressure generated when the PMUT cell is excited with 1V in water.

The piezo-patterned PMUT structure was simulated using the finite element analysis software COMSOL Multiphysics. The material properties used in the simulation are in Table II. The average pressure generated on the membrane surface of the PMUT when it was coupled to water and excited with a 1 V signal is plotted in Figure 2, showing a maximum surface pressure of 20.4 kPa at a frequency of 5.9 MHz. The receive performance of the PMUT was also simulated by applying a pressure of 1 Pa to the membrane's surface. The simulated open circuit voltage was 6.2 μV. The effect of residual stress on the membrane was not considered in this study.

The simulated bending profile of the membrane at resonance is shown in Figure 3. The simulated profile approximates closely that of the bending of a disk with clamped edges, shown as red dashed line.

B. Linear Array

The design of the PMUT linear array is shown in Figure 4. Twenty-two cells in a row are connected in parallel to form one element. The array consists of 96 elements. As per the CSOI design rule, the minimum dead space between the edges of cavities has to be at least 20 μm. Therefore, the pitch between

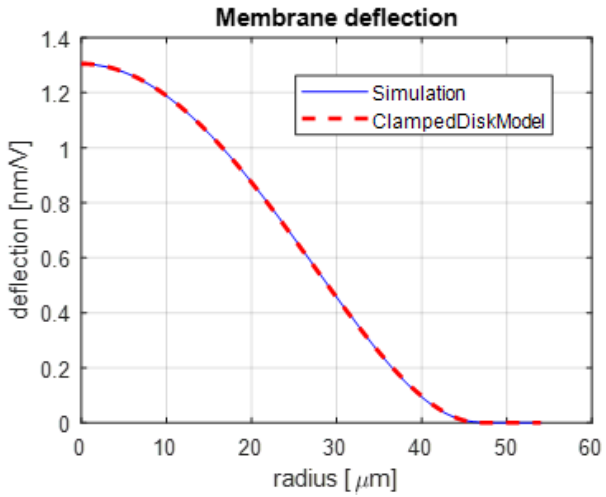

Fig. 3. Simulated deflection profile of the pMUT cell of Fig. 2 (blue line) and fit to lowest order deflection mode of a circular disk with clamped edge $x = x_0(1-(r/r_0)^2)^2$ (red dashed line).

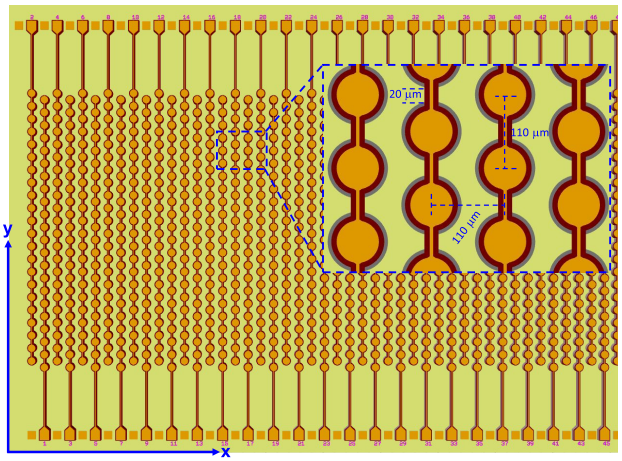

Fig. 4. Design of the PMUT linear array (only a portion of the array is shown here) with piezo layer patterned (maroon) and top electrode patterned (orange).

cells is set to 110 μm (diameter + dead space) in both the X and Y direction. The zig-zag arrangement of rows helped to achieve higher than 20 μm dead space between PMUTs and is expected to reduce the cross-talk between the rows.

The pressure field generated by the array was calculated using an analytical model developed in Matlab. While COMSOL-based PMUT array models are known for their accuracy [20], they are computationally intensive and time-consuming. Nonetheless, the analytical model yielded results that were consistent with actual measurements. In the calculation, it was assumed that 42 elements are connected in parallel. Each PMUT cell was assumed to move in phase with average amplitude 0.4684 nm/V, obtained from COMSOL simulation at resonance. The pressure generated by each drum at the field point was then calculated using far-field approximation of a clamped disk in lossless medium. The results were summed for all radiators (assumed identical). We used the following directivity function for a single cell [21][1]

$$p \propto 6(J_1(\alpha)(2(2/\alpha)^5 - (2/\alpha)^3) - 2J_0(\alpha)(2/\alpha)^4), \qquad (1)$$

[1]Note the misplacement of the factor 6 in Eq. (28) of Ref. [21].

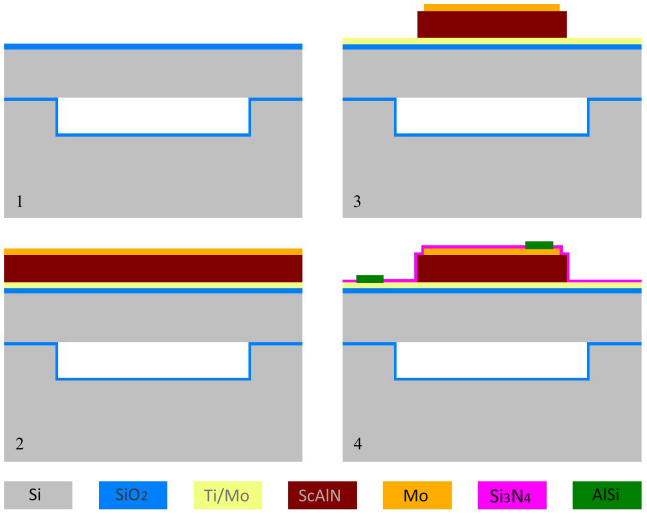

Fig. 5. ScAlN PMUT fabrication process flow: (1) CSOI wafer with thin thermal oxide grown, (2) Sputter deposition of Ti/Mo bottom electrode, ScAlN piezo layer and top Mo electrode, (3) Patterning and etching of Mo top electrode and piezo layer, (4) Deposition and patterning of the nitride passivation layer and AlSi(1%) bond pad.

where $J_i, i = 0, 1$ are the Bessel functions of the first kind, $\alpha = kr_0 \sin\theta$, where $k = 2\pi/\lambda$, r_0 is the drum radius, and θ is the angle between the z-axis and the field point. This approximation is valid when the distance from the drum centre to the field point is much larger than $r_0 = 45$ μm. Minimum z-distance from the transducer used in the calculation was 2 mm. In addition, the far-field limit for a single drum is given approximately by $4r_0^2/\lambda = 30\mu$m. Thus the use of approximation (1) is justified.

The pressure field in the yz-plane (at $x = 0$) when the PMUT array is driven with 3.3-V sinusoidal voltage at 5.7 MHz is plotted in Figure 11(a). In Figure 12(a), the field is calculated at $z = 18$ mm in the xy-plane. According to the yz-field, at $z \simeq 21$ mm the last pressure maximum is obtained, indicating the start of the far field region for the full array. The maximum pressure generated by the array is 53.9 kPa according to the calculation. The transmit sensitivity of the PMUT array was estimated to be around 16.3 kPa/V.

III. Fabrication

PMUTs were fabricated on 6-inch CSOI multi-process wafers provided by Okmetic Oy. The cavity of the PMUT membrane and the device/structural layer are bonded together using fusion bonding to form the CSOI structure, as shown in Figure 5.

The PMUT fabrication process begins with the growth of a thin thermal oxide layer for electrical isolation. The Titanium (Ti)/ Mo bottom electrode, ScAlN piezo active layer and Mo top electrode are sputtered next using the Von Ardenne CS 730 S sputtering system. The thickness of the deposited layers is optimized by measuring with the use of the cross-section SEM (Figure 7). The ScAlN films were deposited using reactive sputtering at a substrate temperature of 450 °C under nitrogen and argon (Ar) atmosphere [22]. Stress calibration was carried out by varying the Ar flow for metal electrodes sputtering and RF bias for ScAlN sputtering.

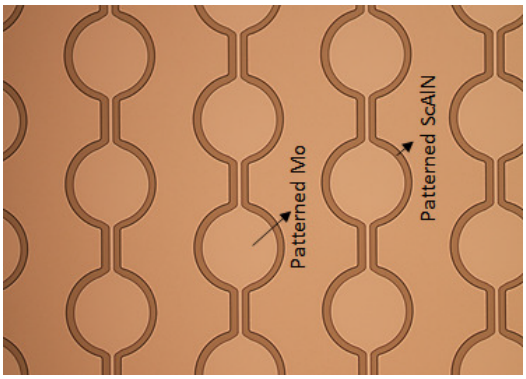

Fig. 6. An optical image of a fabricated PMUT array.

The wafer-level stress variation across a wafer was optimized and was within ±100 MPa. The ScAlN crystal structure was examined using X-ray diffraction techniques. The rocking curve of the ScAlN (002) peak was measured and the full-width half-maximum (FWHM) of the peak was 2.0 ^{0}, indicating good crystallinity of the ScAlN film on Mo.

The PMUTs were fabricated using a simple 4-mask process. The Mo top electrode was patterned and etched first. An oxide mask layer was deposited using the plasma-enhanced chemical vapor deposition (PECVD) system and patterned. The ScAlN piezo layer was wet etched using tetramethyl ammonium hydroxide (TMAH) at 80 °C. Then, the oxide mask layer is removed. Wet etching the ScAlN layer required a longer duration than the AlN and the lateral etching undercut below the mask layer was insignificant in this work, since the patterned piezo layer was a few micrometers wider than the patterned top electrode layer (Figure 6). High-fidelity patterning of ScAlN with the wet etch process under different etch conditions and masks layers was recently studied separately [23]. The effect of piezo layer surface quality before the etch mask deposition process on lateral undercutting during wet etch is discussed here in detail. The ScAlN wet etch process led to the formation and deposition of residues on the wafer surface and the approach we use to reduce this is also summarized [23].

The PMUTs were covered using a thin silicon nitride passivation/protection layer and patterned to open up pad regions for wire bonding. An aluminum-silicon (AlSi(1%)) layer was deposited and patterned on wire bonding contact pads to protect the Mo surface from oxidation [24]. An optical microscope image of part of the fabricated PMUT array is shown in Figure 6. A cross-sectional scanning image of the PMUT membrane is shown in Figure 7. The PMUT device has an 875 nm ScAlN piezo layer sandwiched between the bottom electrode (Ti/Mo: 150 nm) and the top electrode (Mo: 200 nm).

IV. Characterization

A. Electrical Characterization

Fabricated PMUTs, including a 96-element linear array and individual PMUT cells, were electrically characterized in air using a probe station (Cascade Microtech Summit 11000). The measured impedance response and fitted curve of individual PMUT cells in air are shown in Figure 8(a). The electrical equivalent of the PMUT cell was extracted from the impedance response and is shown in the inset. The model fits well with the

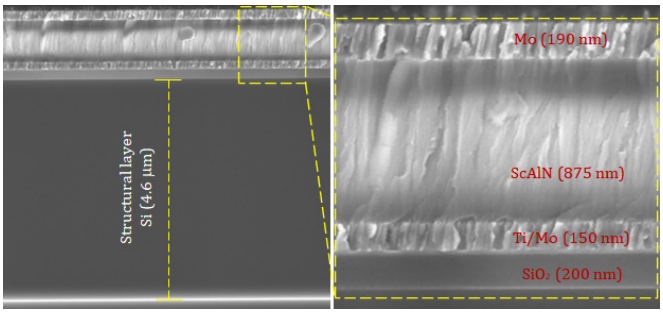

Fig. 7. Cross sectional SEM image of a ScAlN PMUT.

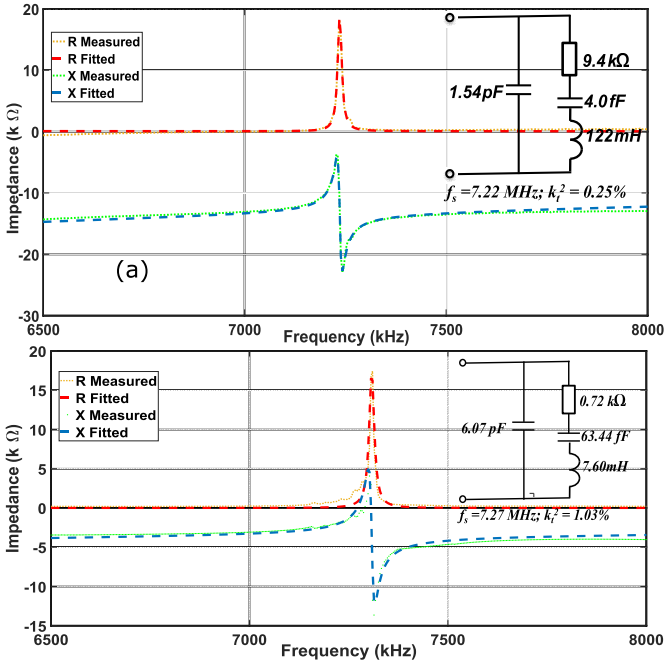

Fig. 8. Impedance plot and BvD model of (a) a PMUT cell (b) PMUT row.

measured data. The resonance frequency of the PMUT in air is around 7.2 MHz. The derived capacitance of the PMUT cell, after subtracting the offset capacitance due to the connection pad and line, is 0.34 pF. From the PMUT cell capacitance and the measured dimensions, the dielectric constant of ScAlN is estimated to be 12. The coupling coefficient (k_t^2) is derived from the series (f_s) and parallel resonance frequency (f_p), and is found to be 0.25%.

The wafer-level electrical characterization of a PMUT linear array was carried out. The measured and fitted impedance response of one PMUT row (element) and the BvD model derived from the impedance response is shown in Figure 8(b). The observed differences between the measured and fitted responses can be attributed to the high resistance of the Mo top electrode and minor structural variations among individual PMUT membranes in the row. The k_t^2 is in the range of 1%. All 96 elements in a PMUT array and 15 different arrays across the wafers were characterized. More than 96% of the measured rows were functional. The average resonance frequency of PMUTs at different wafer locations are shown in Figure 9. The resonance frequency of the PMUT array at the center was slightly higher than the PMUTs at the edges. This variation is due to the Si device layer thickness variation.

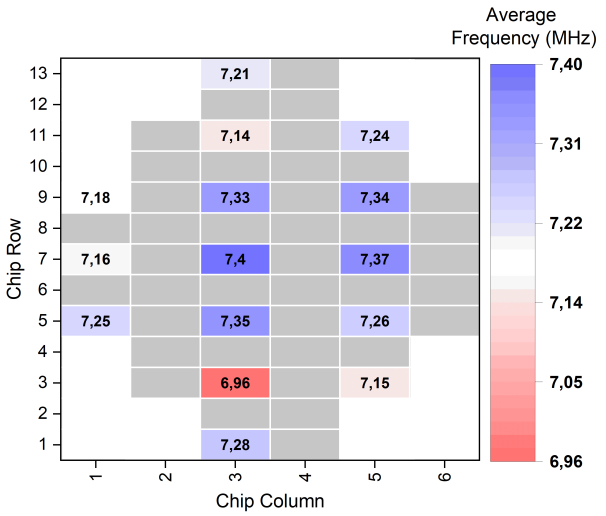

Fig. 9. Average resonance frequency of PMUT across a multi-process 6-inch wafer.

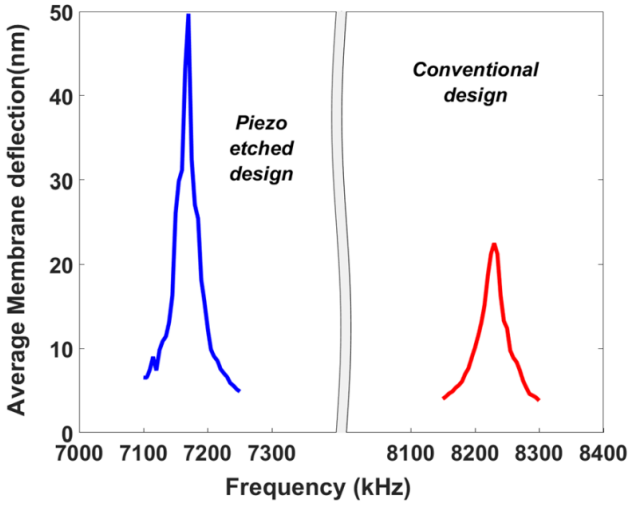

Fig. 10. Average deflection per voltage of ScAlN PMUT cells (left) Piezo etched design. (right) Conventional design.

The frequency variation within an array and the average frequency variation across the wafer is 3% and 6%, respectively. As expected, the piezo patterned water-coupled PMUT showed very good wafer and chip level uniformity. As this variation is much lower compared to the bandwidth of the PMUTs, this will not affect the PMUT performance when used in applications. From these results, it can be concluded that the developed fabrication process has a high yield and as expected piezo patterning does not reduce the wafer-level uniformity.

B. Mechanical Characterization

The static and dynamic membrane deflections of the fabricated PMUT cell were measured using Lyncee Tec's Digital Holographic Analyzer. Static deflection of the patterned and non-patterned conventional PMUTs were measured without applying any excitation voltage to the PMUT. Maximum displacement at the center of patterned PMUT is 150 nm which is only 50 nm, higher than non-patterned PMUT. This showed that the additional stress introduced due to patterning is negligible in the proposed water-coupled PMUT design. Dynamic membrane deflections of piezo-patterned and conventional design when both the PMUTs were excited by a 1 V AC signal is measured and plotted in Figure 10. As expected, the average deflection of the piezo-etched design is two times higher than the conventional PMUT design. The lower frequency of the piezo-patterned PMUTs is due to the lower membrane stiffness.

C. Acoustic Characterization

The transmit and receive performance of the PMUT linear array was measured using Onda's AIMS III acoustic characterization setup. The diced PMUT linear array was placed on a PCB. Forty-two (out of 96) rows in the linear array were connected in parallel by wire bonding it to the PCB. The active area of the PMUT is 2.455 × 4.730 mm. The area is selected based on the requirements of pressure measurement patch. The wire bonds were protected by using the epoxy coating. In the PMUT array design and during the coating process, special

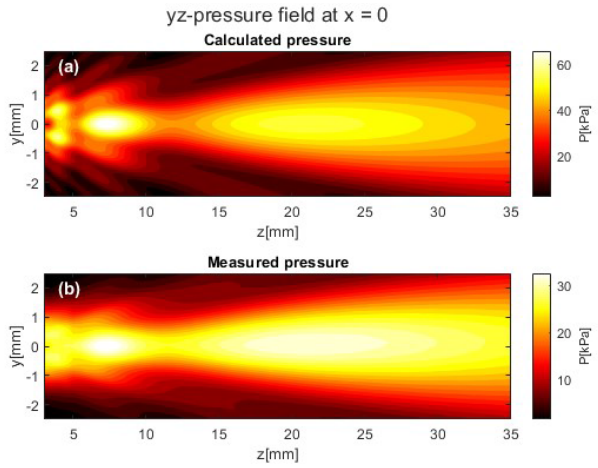

Fig. 11. Contour plot of the pressure field in yz-plane when $x = 0$. (a) calculated (b) measured. The origin is at the centre of the array surface and z is the distance from the xy-plane on which the array surface is located.

care was taken to avoid the overflow of epoxy into the active area of the PMUT. The PMUT array, along with the PCB, is then passivized using synthetic rubber coating (Electrotube LTE [25]) with a thickness of 25 μm.

To measure the transmit performance, the PMUT linear array (along with the PCB) was immersed in a scanning tank filled with DI water. The 42 elements in the PMUT linear array were excited by connecting it to the function generator. A 400 μm diameter hydrophone (Onda's HGL-0400 [26]) was used to measure the pressure generated by the PMUT array. The hydrophone was attached to a 3D motorized moving stage of the characterization setup. The output of the hydrophone was connected to an oscilloscope through a preamplifier. Onda's Soniq software reads, analyzes, and plots the hydrophone data. The hydrophone was kept at the far-field and the resonance frequency of the fabricated PMUT array in water was determined by manually varying the drive frequency. The maximum pressure was recorded at 5.6 MHz. The resonance frequency was close to the simulated values. The acoustic center (where pressure was at the maximum) of the PMUT array was determined by scanning the hydrophone.

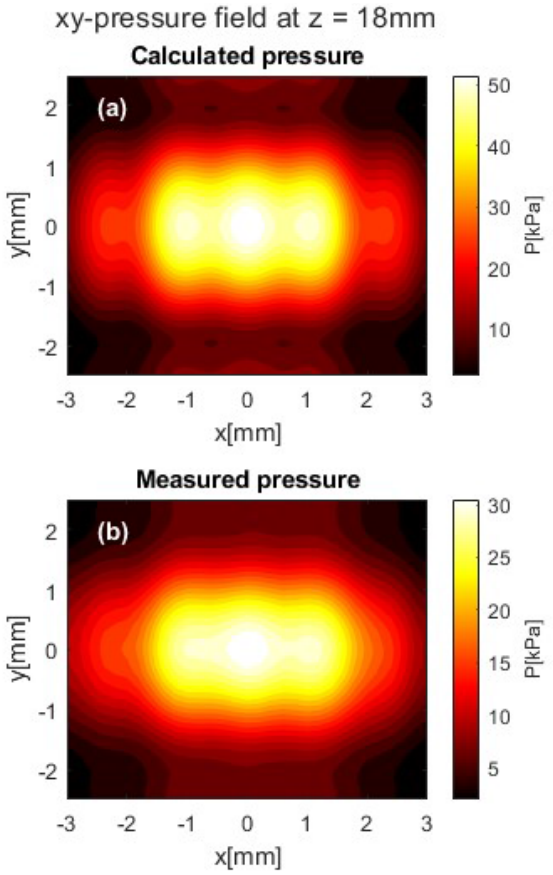

Fig. 12. Contour plot of the pressure field in xy-plane when $z = 18$ mm. (a) calculated (b) measured.

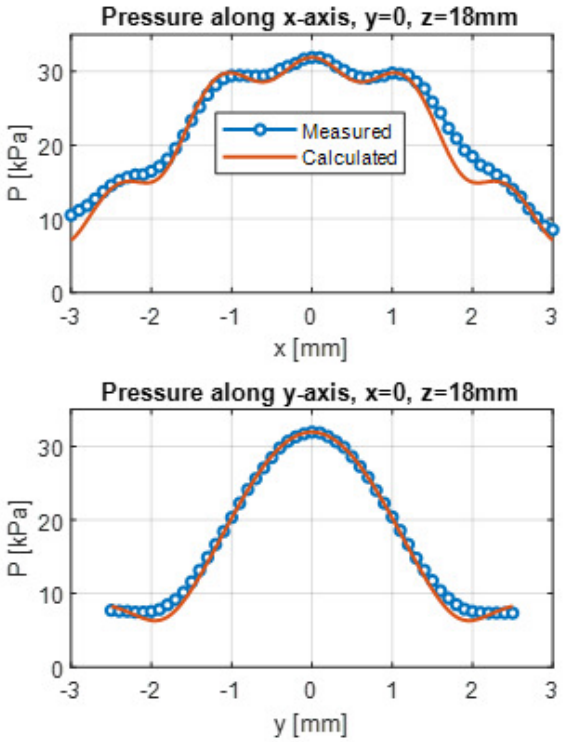

Fig. 13. Comparison of measured and calculated pressure at $z = 18$ mm along the x-axis (upper plots) and along the y-axis (lower plots). The curves are calculated from the data in Figure 12, setting either y or x to zero.Theoretical curves are multiplied by 0.5925 to match maximum in measured curves.

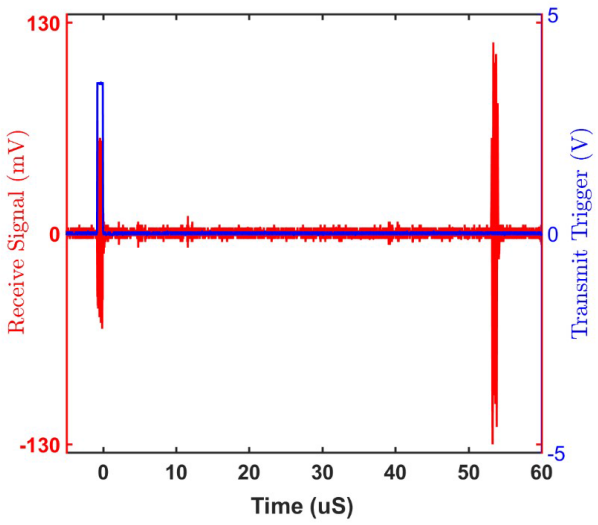

Fig. 14. Voltage generated by the PMUT when operated in Rx mode.

To measure the pressure field, the PMUT was excited with sinusoidal signal (3.3V, 5.7 MHz, 4 cycles). The field generated by the PMUT was measured by scanning the hydrophone in X, Y and Z directions. The field generated in the yz-plane (when $x = 0$) is shown in Figure 11(b). The field generated in the xy-plane at $z = 18$ mm is shown in Figure 12(b). The measured and calculated transmit performances are compared in Fig. 13 and the agreement is reasonably good. As expected, the measured values are somewhat $\sim$40 % lower than the theoretical values, and the finest details are not fully captured in the measurement. The averaging effect is emphasized in the near-field region of the measured pressure map along the yz-plane, shown in Figure 11. The differences are most likely due to several factors, including electrical and mechanical losses in the PMUT cells, the scatter in the transmit properties of the PMUT cells, the finite aperture of the hydrophone used (0.4-mm) averaging the pressure signal, and the sparser sampling of the measured pressure map. Nevertheless, the shape and width of the calculated main lobe are remarkably well reproduced by the measurement.

Maximum pressure with sinusoidal input of 3.3 V, 32.6 kPa, was obtained at $z = 21.5$ mm. This corresponds to transmit sensitivity of 12.6 kPa/V assuming a square input signal. The -3dB bandwidth, which was calculated based on the impulse response, was found to be 2.6 MHz.

To measure receive performance, the ScAlN PMUT was kept 80 mm from a transmitter. One of VTTs AlN PMUT arrays was used as a transmitter. The size of the transmitter PMUT was much larger than the active area of receiver PMUT in the test. This ensures that the pressure field on the receiver PMUT is uniform. The pressure generated by the transmitter PMUT at 80 mm recorded by the hydrophone was 8 kPa. The receiver PMUT was connected to a buffer amplifier. The gain of the amplifier was set to 22. The output of the amplifier is shown in Figure 14. The receive sensitivity calculated from the amplifier output and surface pressure was 1.1 V/MPa.

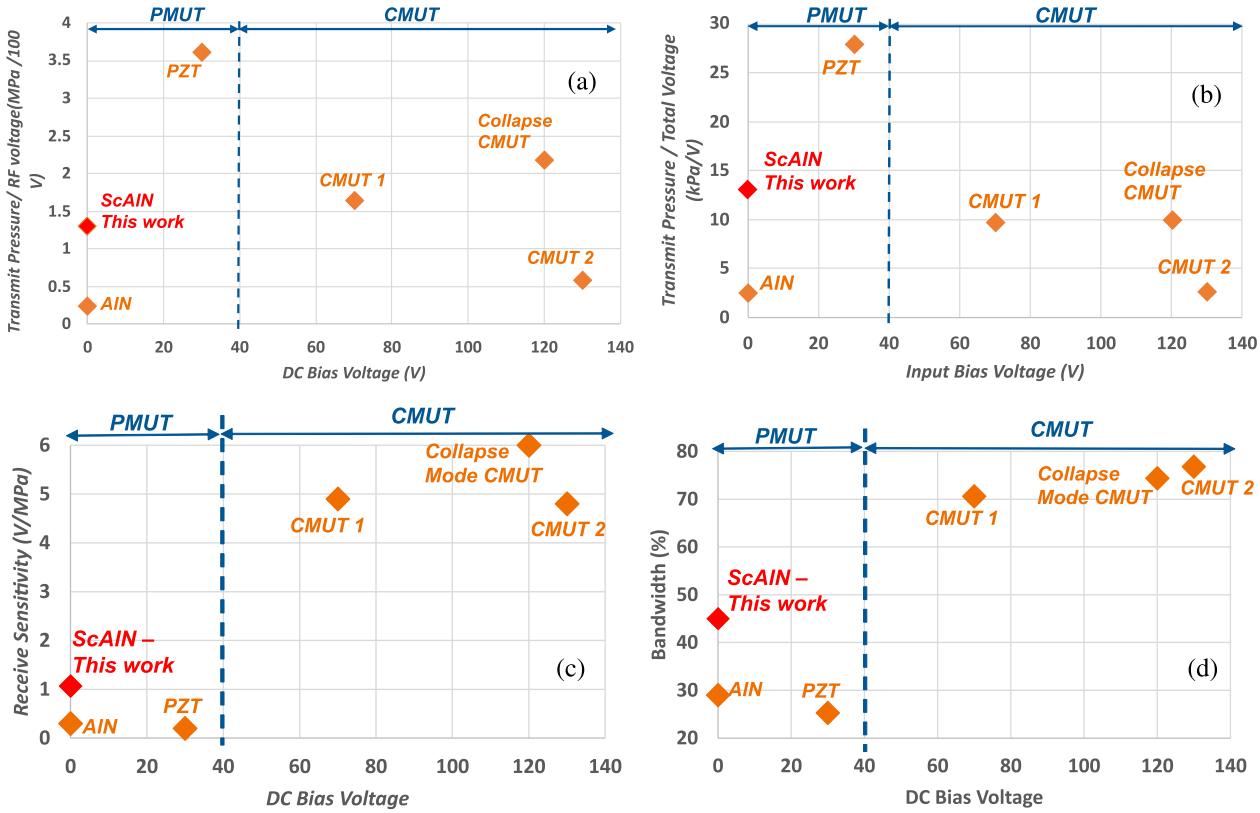

Fig. 15. (a) Transmit pressure generated per RF voltage (b) Transmit Pressure generated per total voltage (RF+DC voltage) (c) Receive Sensitivity (d) bandwidth of different types of MUTs.

V. Discussion - Potential of *ScAlN* PMUTs

Different types of PMUTs and CMUTs are developed by researchers around the globe. As these MUTs are developed for specific applications, they are of different specifications (such as dimensions, frequency, etc). This makes it difficult to compare and identify the benefits and drawbacks of various MUT technologies. In [27], a pan-European benchmarking of MUTs developed using different technologies is carried out. Various types of PMUTs and CMUTs of the same dimensions and frequency range were developed and characterized. The specification of the ScAlN PMUT array discussed in this paper is similar to the high frequency (HF) MUTs used in the benchmarking. The performance of the ScAlN in comparison to the HF benchmarking results is presented. Even though the specification and test setup used in this study and the benchmark study are similar, they are not the same. Some of the main differences are: (1) Elevation of the ScAlN PMUT in this work is 2.5 mm, whereas the specification of benchmarking HF PMUTs is 5 mm; (2) the passivation layer used in this study and benchmarking evaluation are different; (3) the hydrophone and characterization setup used in this study are different; (4) and in this work, receiver sensitivity is calculated from pitch-catch measurement, whereas in the benchmarking study, a pulse-echo technique is used.

The acoustic performances of different MUT technologies are plotted in Figure 15. The bias voltage required for the optimum operation of MUTs varies between 0 and 130V. The performances are plotted against DC bias voltage. Transmit pressure per RF (Square) voltage generated by different types of MUTs is shown in Figure 15(a). The PZT PMUT showed the best transmit performance. The ScAlN PMUT generated output pressure comparable to CMUTs (even if the active area is smaller). One of the main benefits of ScAlN and AlN PMUTs is that they can operate without any DC bias voltage. CMUTs require DC voltages in the range of 70 to 130 V for its operation. Transit pressure generated per total voltage (DC+RF voltage) is plotted and shown in Figure 15(b). In this case, ScAlN PMUT showed better transmit performance than CMUT. The receive performance of various types of MUT is shown in Figure 15(c). The ScAlN PMUT discussed here showed the best receive performance among the PMUTs. Even though PZT PMUT showed very good transmit performance, the receive sensitivity is poor. CMUTs showed better receive performance than PMUTs but at the expense of high DC voltage. The ability of ScAlN and AlN to receive ultrasound without any voltage signal makes it attractive for many applications, like energy harvesting. In bandwidth, the ScAlN PMUT developed in this work shows the best performance in PMUTs, as seen in Figure 15(d). The good transmit-receive performance along with its ability to operate without any DC bias voltage makes the ScAlN PMUT the best choice for applications like wearables, implantables, etc.

Compared to other technologies, ScAlN PMUT is relatively new, and its full potential is yet to be explored. Some of the ongoing works to further improve ScAlN PMUT performance are discussed here. The ScAlN film used for the PMUT fabrication in this work was deposited using an old sputter deposition tool and process. ScAlN sputter deposition technology has now further matured, and the latest systems can now deposit ScAlN films with improved film

thickness uniformity, stress control, high scandium content, piezo quality, etc. PMUTs fabricated using these films could further improve the transmit and receive performance. In the fabricated ScAlN PMUTs, Mo is used as the top electrode. Replacing Mo top electrode with a low resistance electrode material like Al would reduce the resistance losses. Al as the top electrode for ScAlN PMUT increases the complexity of the fabrication; however, this will further improve the PMUT performance. The patterning of the bottom electrode could reduce the offset capacitance and thereby improves the receive sensitivity. Patterning the bottom electrode before ScAlN film deposition may affect the piezo quality and increase stress variation. Process development for depositing high-quality ScAlN films on the patterned bottom electrode is ongoing.

VI. Conclusion

The development of a ScAlN PMUT linear array used in a blood pressure monitoring patch is discussed in this paper. PMUTs, both single-cell and linear array, were designed, and their performances were initially evaluated using simulation models. The patterning of the ScAlN piezoelectric layer improved the PMUT performance. A simple 4-mask fabrication process for the development of a piezo-patterned ScAlN PMUT was developed. Electrical characterization of the PMUT showed that the CSOI-based fabrication process for ScAlN PMUT has a very good yield. Acoustic characterization was carried out to evaluate the performance of the linear arrays. The measurement results are comparable to the results obtained from the simulation models. The ScAlN PMUT showed good transmit sensitivity, receive sensitivity and wide bandwidth. Comparison with state-of-the-art MUT technologies showed that ScAlN PMUTs are the best choice for voltage-limited medical applications.

Acknowledgment

The authors would also like to thank Stefan Mertin, Harri Pohjonen, Kirsi Järvi, and Paula Holmlund.

References

[1] J. Wang, Z. Zheng, J. Chan, and J. T. W. Yeow, "Capacitive micromachined ultrasound transducers for intravascular ultrasound imaging," *Microsyst. Nanoeng.*, vol. 6, no. 1, pp. 1–13, Aug. 2020.

[2] T. Otake, H. Tanaka, A. Sako, M. Fukada, K. Imagawa, and M. Sato, "Development of 4G CMUT (CMUT linear SML44 probe)," *Adv. Ultrasound Diagnosis Therapy*, vol. 4, no. 4, pp. 379–382, 2020.

[3] *Butterfly Network*. Accessed: Mar. 30, 2022. [Online]. Available: https://www.butterflynetwork.com/

[4] A. S. Savoia, R. Matera, F. Quaglia, and S. Ricci, "A feasibility study of a PMUT-based wearable sensor for the automatic monitoring of carotid artery parameters," in *Proc. IEEE Int. Ultrason. Symp. (IUS)*, Sep. 2021, pp. 1–4.

[5] S. Sun et al., "Eye-tracking monitoring based on PMUT arrays," *J. Microelectromech. Syst.*, vol. 31, no. 1, pp. 45–53, Feb. 2022.

[6] B. Herrera, F. Pop, C. Cassella, and M. Rinaldi, "AlN PMUT-based ultrasonic power transfer links for implantable electronics," in *Proc. 20th Int. Conf. Solid-State Sensors, Actuators Microsyst. Eurosensors*, Jun. 2019, pp. 861–864.

[7] Y. Lu and D. A. Horsley, "Modeling, fabrication, and characterization of piezoelectric micromachined ultrasonic transducer arrays based on cavity SOI wafers," *J. Microelectromech. Syst.*, vol. 24, no. 4, pp. 1142–1149, Aug. 2015.

[8] L. Wang, W. Zhu, Z. Wu, W. Liu, and C. Sun, "A novel coupled piezoelectric micromachined ultrasonic transducer based on piston mode," *IEEE Trans. Ultrason., Ferroelectr., Freq. Control*, vol. 68, no. 11, pp. 3396–3405, Nov. 2021.

[9] D. E. Dausch, K. H. Gilchrist, J. B. Carlson, S. D. Hall, J. B. Castellucci, and O. T. von Ramm, "In vivo real-time 3-D intracardiac echo using PMUT arrays," *IEEE Trans. Ultrason., Ferroelectr., Freq. Control*, vol. 61, no. 10, pp. 1754–1764, Oct. 2014.

[10] R. Matloub et al., "Piezoelectric $Al_{1-x}Sc_xN$ thin films: A semiconductor compatible solution for mechanical energy harvesting and sensors," *Appl. Phys. Lett.*, vol. 102, no. 15, Apr. 2013, Art. no. 152903.

[11] G. Giribaldi, B. H. Soukup, P. Simeoni, L. Colombo, and M. Rinaldi, "Matching network-boosted 36% ScAlN pMUT linear array," in *Proc. IEEE 35th Int. Conf. Micro Electro Mech. Syst. Conf. (MEMS)*, Jan. 2022, pp. 251–254.

[12] Q. Wang, Y. Lu, S. Mishin, Y. Oshmyansky, and D. A. Horsley, "Design, fabrication, and characterization of scandium aluminum nitride-based piezoelectric micromachined ultrasonic transducers," *J. Microelectromech. Syst.*, vol. 26, no. 5, pp. 1132–1139, Oct. 2017.

[13] C. Wang et al., "Monitoring of the central blood pressure waveform via a conformal ultrasonic device," *Nature Biomed. Eng.*, vol. 2, no. 9, pp. 687–695, Sep. 2018.

[14] T. Powałowski and B. Peńsko, "A noninvasive ultrasonic method for the elasticity evaluation of the carotid arteries and its application in the diagnosis of the cerebro-vascular system," *Arch. Acoust.*, vol. 13, nos. 1–2, pp. 109–126, 1988.

[15] Y. Liang, B. Eovino, and L. Lin, "Piezoelectric micromachined ultrasonic transducers with pinned boundary structure," *J. Microelectromech. Syst.*, vol. 29, no. 4, pp. 585–591, Aug. 2020.

[16] T. Wang, T. Kobayashi, and C. Lee, "Highly sensitive piezoelectric micromachined ultrasonic transducer operated in air," *Micro Nano Lett.*, vol. 11, no. 10, pp. 558–562, Oct. 2016.

[17] C. B. Karuthedath, A. T. Sebastian, J. Saarilahti, T. Sillanpaa, and T. Pensala, "Design and fabrication of aluminum nitride piezoelectric micromachined ultrasonic transducers for air flow measurements," in *Proc. IEEE Int. Ultrason. Symp. (IUS)*, Oct. 2019, pp. 2489–2492.

[18] G. Ross, H. Dong, C. B. Karuthedath, A. T. Sebastian, T. Pensala, and M. Paulasto-Kröckel, "The impact of residual stress on resonating piezoelectric devices," *Mater. Des.*, vol. 196, Nov. 2020, Art. no. 109126.

[19] C. Baby Karuthedath, A. Thanniyil Sebastian, T. Sillanpää, and T. Pensala, "Passive temperature compensation of piezoelectric micromachined ultrasonic transducers (PMUTs)," in *Proc. IEEE Int. Ultrason. Symp. (IUS)*, Oct. 2022, pp. 1–4.

[20] O. M. O. Abdalla, G. Massimino, A. S. Savoia, F. Quaglia, and A. Corigliano, "Efficient modeling and simulation of PMUT arrays in various ambients," *Micromachines*, vol. 13, no. 6, p. 962, Jun. 2022.

[21] D. L. Dekker, R. L. Piziali, and E. Dong, "Effect of boundary conditions on the ultrasonic-beam characteristics of circular disks," *J. Acoust. Soc. Amer.*, vol. 56, no. 1, pp. 87–93, Jul. 1974, doi: 10.1121/1.1903238.

[22] E. Österlund et al., "Stability and residual stresses of sputtered Wurtzite AlScN thin films," *Phys. Rev. Mater.*, vol. 5, no. 3, Mar. 2021, Art. no. 035001.

[23] K. Airola et al., "High-fidelity patterning of AlN and ScAlN thin films with wet chemical etching," *Materialia*, vol. 22, May 2022, Art. no. 101403.

[24] K. Bespalova et al., "Characterization of AlScN-based multilayer systems for piezoelectric micromachined ultrasound transducer (pMUT) fabrication," *J. Microelectromech. Syst.*, vol. 30, no. 2, pp. 290–298, Apr. 2021.

[25] Electrolube. (2016). *LTC Aromatic Free Low Temperature Coating*. [Online]. Available: https://electrolube.com/product/ltc-low-temperature-conformal-coating/

[26] Onda Corp. (2020). *HDL Hydrophones*. [Online]. Available: https://www.ondacorp.com/images/brochures/Onda_HGL_DataSheet.pdf

[27] ECSEL Joint Undertaking project POSITION-2. (Nov. 2021). *A European MEMS Ultrasound Benchmark*. [Online]. Available: http://position-2.eu/wp-content/uploads/CMUT-PMUT-Benchmark-Technical-Whitepaper.pdf